Evolving loop structure in gradually tilted two-dimensional granular packings

Ashley G. Smart[*] and Julio M. Ottino

Department of Chemical and Biological Engineering, Northwestern University, 2145 Sheridan Road, Evanston, Illinois 60208, USA

Granular packings, especially near the jamming transition, form fragile networks where small perturbations can lead to destabilization and large scale rearrangements. A key stabilizing element in two dimensions is the contact loop, yet surprisingly little is known about contact loop statistics in realistic granular networks. In this paper, we use particle dynamics to study the evolution of contact loop structure in a gradually tilted two-dimensional granular bed. We find that the resulting contact loop distributions (1) are sensitive to material properties, (2) deviate from the expected structure of a randomly wired lattice, and (3) are uniquely dependent on tilting angle. Also, we introduce a quantitative measure of loop stability ξ and show that increased tilting results in a gradual destabilization of individual loops. We briefly discuss the considerations for extending our approach to three dimensions.

I. INTRODUCTION

Granular materials constitute a unique and complex class of matter. Under a confining stress, granular matter adopts an unusual solidlike state (i.e., a granular packing) marked by heterogeneity [1–3], self-organization [4,5], stress memory [6], and a stress response that is neither entirely elastic nor entirely plastic [7,8]. A fundamental grasp of such granular behavior is both practically and theoretically important, yet surprisingly elusive.

A hallmark of granular packings—especially at the jamming transition, or isostatic limit—is fragility [9]. That is, they respond elastically only to compatible loads; incompatible loads lead to plastic reorganizations [4]. This fragile behavior is, arguably, a result of the jamming process itself and attributable to the formation of unstable force chains [4,10]. It can therefore be argued that fragility arises from mesoscale structural motifs—unstable contact chains on the order of several particles in length. But other mesostructures—in two dimensions, contact loops—are mechanically robust; they can support a finite range of compatible loads.

Contact loops are known to contribute to granular stability [11,12], and have inspired new approaches to understanding the stress response of granular matter. Some theoretical models employ contact loops, not grains, as the basic structural units [13–15]. However, surprisingly little is known about the statistics of contact loops in realistic granular packings. Several questions remain open. Which loop sizes are most prevalent? How does loop structure depend on material properties? How and when do loops destabilize and deform?

In this paper, we investigate loop structure in simulated 2D granular packings. We investigate the influence of surface roughness by varying interparticle friction coefficients and investigate structural evolution in the approach to the unjamming transition by varying the tilt angle. We find that contact loop distributions are (1) sensitive to material properties, (2) deviate from the expected structure of a randomly wired lattice, and (3) are uniquely dependent on tilting angle. Also,

we introduce a quantitative measure of loop stability ξ and show that increased tilting results in a gradual destabilization of individual loops. We conclude with a brief discussion of considerations for extending our approach to three dimensions.

Contact loops as stabilizing elements

A granular packing can be viewed as a collection of mesoscale contact structures called "contact loops." These loops are significant in that they are the smallest structural arrangements that can support two-dimensional perturbations of a compressive load, as illustrated by the following example.

Consider three rigid particles arranged in a straight line (friction is unimportant). The contact forces f_{12} and f_{23} define the external compressive forces f_a and f_c exerted at either end (see Fig. 1). Any orientational perturbation of the external compressive force results in what is known as an incompatible load—given the linear contact arrangement, there is no combination of f_{12} and f_{23} that can balance even
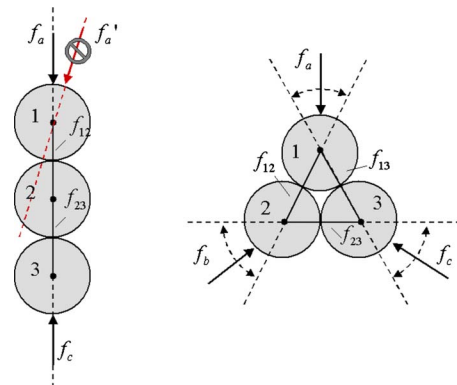

FIG. 1. (Color online) Contact loops as stable mesostructures. A linear contact structure (f_{12}, f_{23}) can support linear compression (f_a, f_b). However, any 2D perturbation of the compressive force (e.g., f_a') yields a load that is incompatible with the linear contact structure. For this reason we say that contact chains are locally fragile. On the other hand, contacts arranged in a triangular loop can support various compressive loads f_a, f_b, and f_c.
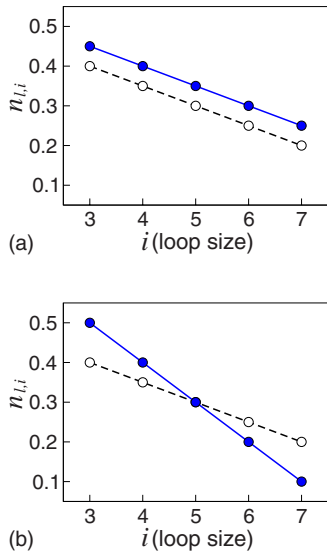
*a-smart@northwestern.edu

FIG. 2. (Color online) Relationships between loop distributions and packing stability. In (a) the solid curve represents a network with a higher overall density of contact loops; in (b) a network with a high relatively density of smaller loops, as compared to the dashed curve. In both cases, the solid curve represents the more stable loop distribution.

a slight change in the direction of one of the externally applied forces. Such a perturbation would cause the linear contact structure to buckle—the structure is said to be fragile (a more rigorous discussion of this example can be found in Ref. [10]).

Now consider the same particles arranged in a triangular loop, with contact forces f_{12}, f_{23}, and f_{13}. Specifically, we say that the arrangement is a third-order loop, where the order indicates the number of particles or contacts that comprise the loop. Again, the contact structure defines a set of external compressive forces f_a, f_b, and f_c. In this case, however, an orientational perturbation can be balanced by an adjustment of the remaining forces (f_{12}, f_{23}, and f_{13}) without deforming the contact structure. In fact, we can define a finite range of compatible loads (the contact loop has an infinite number of compatible arrangements, whereas the contact line has only one). Furthermore, if any particle is removed from the loop, it becomes unstable to perturbation. The same is true for larger contact loops and lines.

The above example suggests that contact loops contribute to network stability—they can be viewed as the building blocks that comprise a mechanically stable network. It can also be inferred that loop stability decreases with increasing loop order (consider that an infinitely large loop is essentially a linear chain). From these conclusions, we expect the following trends—everything else equal—to hold true: (1) networks with high loop density are more stable (less fragile) than those with low loop density [see Fig. 2(a)] and (2) networks rich in lower order loops are more stable than those rich in higher order loops [see Fig. 2(b)]. Here, we have defined loop density $n_{l,i}$ as

$$n_{l,i} = N_{l,i}/N_n, \qquad (1)$$

where i is the loop order (number of particles in the loop), $N_{l,i}$ is the number of loops of order i, and N_n is the total

number of particles. Assumptions (1) and (2) above—although not essential to the following discussion—help to aid our interpretation of contact loop distribution data.

II. METHODS

A. Particle dynamics

We simulate two-dimensional systems of rough disks using particle dynamics (PD)—normal contact forces are calculated using the linear-spring dashpot model [16], and tangential forces are calculated using the Cundall and Strack model [17]. The relevant dimensionless quantity describing particle stiffness is σ,

$$\sigma = \frac{mg}{2k_n r}, \qquad (2)$$

where m is particle mass, g is gravity ($=9.8$ m/s^2), k_n is the normal spring force constant, and r is particle radius. σ gives the dimensionless deformation per unit particle weight, so that a particle resting under its own weight has contact deformation equal to σr. For our simulations, particles are relatively stiff, with $\sigma \approx 5 \times 10^{-4}$.

Packed beds are generated in a three stage process. First, in the initiation stage, N_n point particles, with initial diameters equal to zero, are placed at random inside a box of prescribed width L_x and height L_y. Next, in the growth stage, particles grow to their prespecified sizes—growing particles can collide, transferring small amounts of kinetic energy through dissipative collisions. (These first two stages are similar, in spirit, to the Lubachevsky-Stiller method of producing random packings [18].) The final stage is a sedimentation stage—gravity is introduced and particles are allowed to settle, under their own weight, into a packed state [see Fig. 3(a)].

The final dimensions of the packing approximate a rectangle, with width $w = L_x = 120d$ and bed height $h \approx 20d$, where d is the mean particle diameter ($N_n = 2500$ particles). The horizontal boundary is periodic (no vertical walls), and the floor is infinitely rough, i.e., particles touching the floor are not permitted to move horizontally. Particle diameters are normally distributed with a variance equal to 10% of the mean in order to prevent crystallization. To examine the role of interparticle friction, we considering packings over the range $0 \leq \mu \leq 0.5$, where μ is the Coulomb friction coefficient.

The resulting packings can be viewed as networks: particles are represented as nodes, interparticle contacts are represented as edges, and each edge is weighted according to the normal force f acting along its corresponding contact [see Fig. 3(b)]. A contact loop can then be precisely defined as a path along the granular network that forms a nonintersected circuit. Due to gravity, contact forces tend to increase with depth. We remove this effect by normalizing contact forces with respect to depth:

$$f'_{ij} = \frac{f_{ij}}{h - y_{ij}}, \qquad (3)$$

where y_{ij} is the vertical position of the contact [see Fig. 3(c)]. We approximate the bed height h as
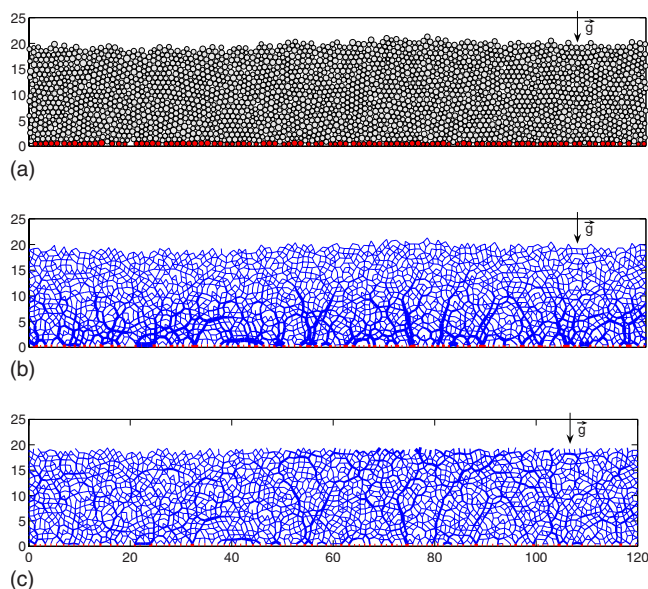
FIG. 3. (Color online) The granular bed as a network. (a) 2500 granular particles are allowed to settle under gravity and come to rest, forming a granular bed about 20 particle diameters deep and 120 particles in length (although the horizontal boundaries are periodic). The layer of particles touching the bed are fixed in place, approximating an infinitely rough floor. (b) The bed can be represented as a network, where each contact is represented by an edge and each edge is weighted according to the normal force along its corresponding contact. Thicker lines near the base indicate a pressure gradient; pressure increases with vertical depth. (c) The same network with edges normalized with respect to depth, so that the average edge weight of a layer is independent of its depth.

$$h = 2 \frac{1}{N_c} \sum y_{ij}, \qquad (4)$$

where N_c is the number of contacts, and the sum is taken over all contact pairs. We exclude the top two layers of contacts—contacts with $(h - y_{ij}) < 2d$—from our analysis, as Eq. (3) may yield highly fluctuating values of f'_{ij} near the surface.

B. Tilting protocol

The tilting protocol begins after particles have been allowed to fully settle and equilibrate in the bed. We fix the orientation of the bed and allow θ_g, the angle of the gravity vector with respect to vertical, to increase in increments (for low tilting rates, this is equivalent to fixing the orientation of gravity and incrementally tilting the bed). The free surface remains horizontal throughout the entire experiment. We alternate two-second tilting intervals (constant rotation rate of 5×10^{-3} rad/s) with two-second rest intervals so that fluctuations caused by tilting can dissipate prior to gathering data (see Fig. 4). We only consider data obtained at or below the marginal angle of stability so that the data and analysis apply to packings in the quasistatic, solidlike regime, not steady or continuous flow.
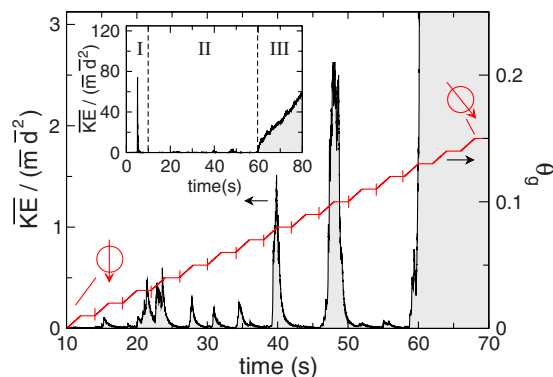

FIG. 4. (Color online) Tilting protocol and kinetic energy profile. θ_g, the angle of the gravity vector with respect to vertical (red curve), is increased incrementally, with each period consisting of a 2-s tilting interval (constant rotation rate of 5×10^{-3} rad/sec) followed by a 2-s rest interval, which allows for dissipation of tilting-induced fluctuations in the kinetic energy (black curve, filled to baseline with gray). Network data is taken at the end of each period (denoted by the vertical notches in the θ_g curve). We have normalized the mean kinetic energy per particle as $\overline{KE}/\overline{m}\overline{d}^2$ so that $\overline{KE}/\overline{m}\overline{d}^2$ has units s^{-2} and a particle with $\overline{KE}/\overline{m}\overline{d}^2 = 1$ has sufficient kinetic energy to move one particle diameter per s. In the inset, the entire kinetic energy profile is shown, including (i) the preparation stage, (ii) the quasistatic tilting regime, and (iii) the steady flow regime. For the purpose of this study, we consider network data obtained in region ii, i.e., data obtained at or below the angle of marginal of stability. The kinetic energy profile shown here is for a single tilting experiment involving smooth particles.

C. Loop-finding algorithm

We use a breadth-first searching algorithm, exploiting the constraints of granular packing geometry to to find contact loops. For each particle, or node i, we identify pairs of adjacent neighbors j and k. Each j-i-k combination then constitutes a part of exactly one contact loop (see Fig. 5). We use a breadth-first searching algorithm to determine the size of the loop: If node j has k as a neighbor the loop is order 3;
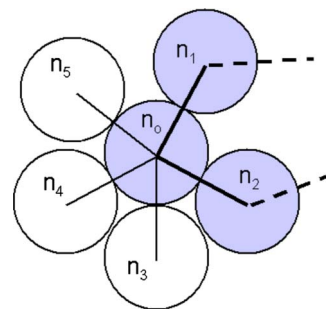

FIG. 5. (Color online) Adjacent neighbors and the loop counting algorithm. For each particle or node, we identify pairs of adjacent neighbors. In this example, n_1 and n_2 are an adjacent neighbor pair of node n_0 (as are n_2 and n_3, n_3 and n_4, and so on). Each node-adjacent node pair combination (here, we have highlighted the n_1-n_0-n_2 combination) then constitutes a part of exactly one contact loop. The total number of contacts, or edges, in the loop is calculated using a breadth-first searching algorithm.
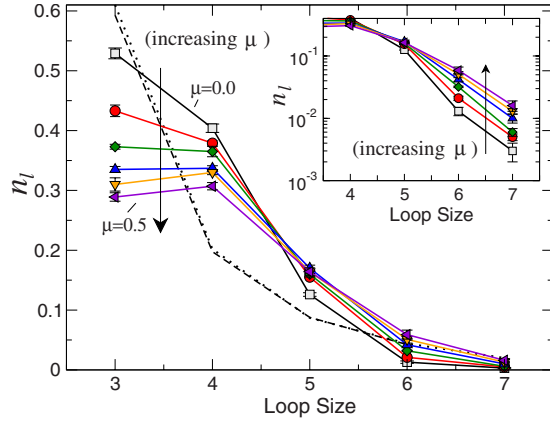
FIG. 6. (Color online) Distributions of contact loops in untilted granular beds. Loop distributions for packings with μ ranging from 0 to 0.5 ($\theta_g=0$). Increasing surface friction corresponds to a decreasing density of low order loops an increasing density of high order loops. The dashed curve is the analytical solution for a randomly wired triangular lattice and the dotted curve is the numerical result from random rewiring of a simulated granular network; both are calculated using $Z=4$ (in the case of the triangular lattice, this means that adjacent nodes on the lattice are connected with a probability $p_e=4/6$).

else, if any neighbor of j (excluding i) has k as a neighbor, the loop is order 4; else if any of second neighbor of j (excluding i and j) has k as a neighbor, the loop is order 5; and so on. We confirm the results with visual checks on small portions of sample networks.

III. CONTACT LOOP STATISTICS

In general, the PD-generated granular networks are richest in third and fourth order loops, with loops as high as seventh order occurring with some, albeit diminishing, regularity (see Fig. 6). The details of the loop distribution vary according to friction properties: networks formed with smoother particles contain more third- and fourth-order loops, whereas networks formed with rough particles are more likely to contain higher order loops. In systems with $\mu<0.3$, third order loops are the most frequently occurring loop size; in those with $\mu>0.3$, fourth order loops occur most frequently. These differences between smooth and rough beds reflect a variation in packing density: smooth particles form densely packed beds—which favor small loops—and rough particles form porous beds—which favor larger loops.

A. Loops in a randomly wired lattice

It is useful to compare loop statistics in the granular packing to the theoretical expectation for a randomly wired lattice. We consider an infinite triangular lattice, with edges placed randomly between neighboring nodes. The probability p_e of finding an edge between any two neighboring node pairs is

$$p_e = \frac{Z}{6}, \qquad (5)$$

where Z is the mean coordination number, or mean number of edges connected to a node ($Z=2N_e/N_n$). It follows that the

probability $p_{l,3}$ that a group of three neighboring particles are connected by a triangular set of edges is equal to p_e^3. Since there are $2N_n$ unique potential triangular arrangements, the expected number of third-order loops is

$$N_{l,3}^{\mathrm{rand}} = 2N_n p_e^3. \qquad (6)$$

It is useful to represent the expected number of loops as a density

$$n_{l,3}^{\mathrm{rand}} = \frac{N_{l,3}^{\mathrm{rand}}}{N_n} = 2p_e^3. \qquad (7)$$

In a similar manner, we can derive $n_{l,4}^{\mathrm{rand}}$. In this case $p_{l,4}$ is equal to $p_e^4(1-p_e)$, and the number of unique potential arrangements is equal to $3N_n$, resulting in

$$n_{l,4}^{\mathrm{rand}} = 3p_e^4(1 - p_e). \qquad (8)$$

Using the same methodology for higher order loops, we obtain

$$n_{l,5}^{\mathrm{rand}} = 6p_e^5(1 - p_e)^2, \qquad (9)$$

$$n_{l,6}^{\mathrm{rand}} = 20p_e^6(1 - p_e)^3 + p_e^6(1 - p_e)^6, \qquad (10)$$

$$n_{l,7}^{\mathrm{rand}} = 36p_e^7(1 - p_e)^4 + 6p_e^7(1 - p_e)^7. \qquad (11)$$

We can also calculate the random loop probability numerically by randomly rewiring the nodes of a PD-generated granular network. To do so, however, requires that we relax the definition of "neighbor pair." In the PD-generated network, neighboring particles are in contact—i.e., the distance between neighboring particle centers α_{ij} is less than or equal to their mean particle diameter $(d_i+d_j)/2$ (this is approximately the same as saying $\alpha_{ij}<d$, where d is mean particle diameter over the entire system). To randomize, we relax this definition slightly, defining "potential neighbors" as nodes for which $\alpha_{ij} \leq 1.2d$. Defined this way, each node typically has about six potential neighbors—corresponding to its immediately surrounding layer of particles.

Using the PD-generated lattice, we connect pairs of potential neighbors at random, starting from the completely unconnected network (no edges) and adding $N_e=N_n(Z/2)$ edges, so that the rewired network has mean coordination number equal to Z. In this way, we construct a network that has identical particle positions as the granular packing, but randomized neighbor connections. From this method, we obtain numerical results that are in good agreement with the analytical solution for nodes on a triangular lattice (compare dashed and dotted curves in Fig. 6).

Loop distributions in PD packings differ significantly from the expected random result, particularly for lower order loops—granular packings tend to have significantly fewer third-order loops and significantly more fourth-order loops than expected from the random model (see Fig. 6). This suggests the influence of force balance constraints—in the lattice model, we assume that nodes are connected to their neighbors with equal probability; in force-constrained networks, certain contact arrangements are statistically more probable than others.
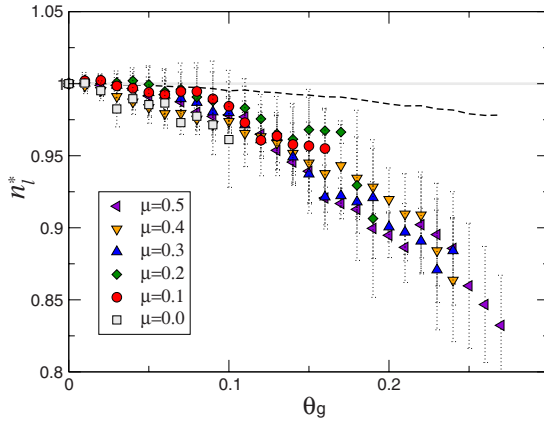
FIG. 7. (Color online) Third order loop density as a function of tilting angle. Relative third order loop density $n_{l,3}^*(\theta_g)$ $=n_{l,3}(\theta_g)/n_{l,3}(\theta_g=0)$ tends to decrease with increasing tilting angle. This decrease is accompanied by a decrease in the mean coordination number Z (denoted by a dashed line).

B. Effects of tilting on loop structure

The dynamics of a tilted bed, even in the quasistatic regime, are complex—new contacts are formed, old contacts are destroyed, and forces along enduring contacts change in magnitude as the bed approaches the unjamming transition. A widely accepted view is that these granule-scale changes conspire to make the bed less resilient to perturbation, i.e., more fragile [9,19]. In other words, a granular packing is most fragile at the unjamming transition (which corresponds with the limit of isostaticity). This view is supported, quantitatively, by the loop analysis results for our tilted bed simulations.

Loop density—particularly $n_{l,3}$—tends to decrease as the tilting angle is increased, suggesting increased fragility (see Fig. 7). However, the decrease in $n_{l,3}$ corresponds with a decrease in mean coordination number Z. A practical question arises: is decreasing loop density in the tilted bed a unique effect of tilting, or a generic consequence of the decreasing contact density (i.e., Z)?

To address this question, we first determine a relationship for $n_{l,3}(Z)$ in untilted beds. From Eq. (7), we expect $n_{1,3} \propto Z^3$. The actual dependence observed in the granular packings is stronger. The data is well described by a fit of the form

$$n_{l,3} = \alpha(Z - \beta)^\gamma, \qquad (12)$$

where the power-law exponent is $\gamma = 3.53 \pm 0.02$ (the fit was generated using $\alpha = 0.13$ and $\beta = 1.39$) [see Fig. 8(a)].

Equation (7), which describes $n_{l,3}(Z)$ as a function of contact density in untilted beds, also approximately describes $n_{l,3}(Z)$ for the various tilting angles. We can then say that the effects of tilting on $n_{l,3}$ are generic—i.e., they cannot be distinguished from contact density effects.

On the contrary, tilting has a unique effect on the fourth-order loop density $n_{l,4}$ [see Fig. 8(b)]. $n_{l,4}$ tends initially to decrease with increasing tilting angle, then—for beds with $\mu \geq 0.2$—increase prior to reaching the marginal angle of stability (a likely explanation is that third-order loops desta-
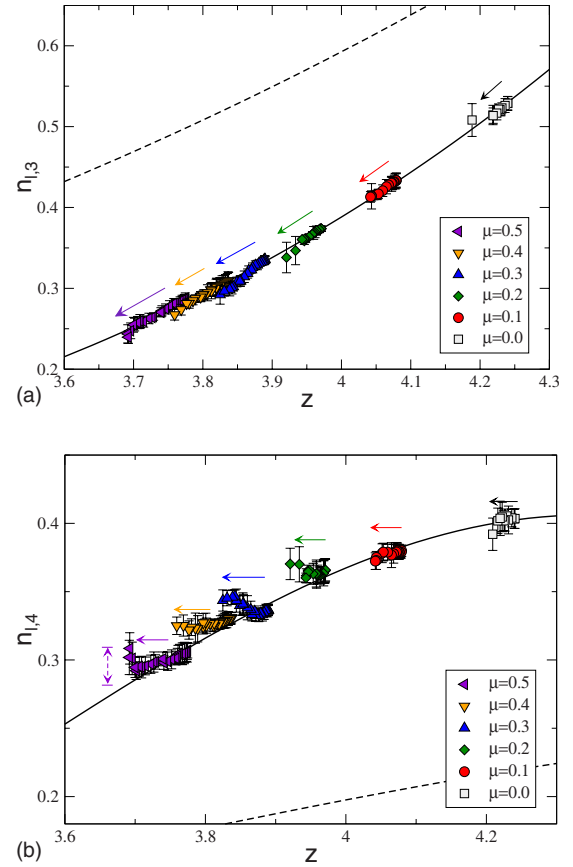

FIG. 8. (Color online) Loop density and coordination number. In (a) and (b), solid curves represent the effect of contact density on loop density—they are best fit regressions of loop densities in untilted beds of various friction coefficients μ. The dashed curves are the theoretical prediction. Filled symbols indicate the evolving loop density as θ_g is increased. For $n_{l,3}$ (a) the data for the tilted bed lie close to the solid curve, suggesting that tilting effects on $n_{l,3}$ are generic (they are indistinguishable from the effects of contact density). For $n_{l,4}$ (b) the data for the tilted bed deviate significantly from the solid curve, indicating that tilting effects on $n_{l,3}$ are unique (they can be distinguished from the effects of contact density).

bilize and become fourth-order loops as the system nears failure). Unlike $n_{l,3}$, the curve that describes $n_{l,4}(Z)$ in untilted beds tends to underestimate the density of fourth-order loops when the bed is tilted. Thus we can say that effects of tilting on $n_{l,4}$ are unique—they are distinguishable from contact density effects.

IV. WEIGHTED CONTACT LOOPS

Loop structures, as described above, are topological constructs; they are defined solely by the number of edges. However, loops with an identical number of edges do not necessarily have identical stability: the magnitude and arrangement of contact forces factor heavily into whether a particular loop will be able to withstand perturbation. Below, we show that relative loop stability can be quantified with a weighting function ξ. We then use ξ to revisit the problem of the tilted bed, constructing a more complete relationship be-
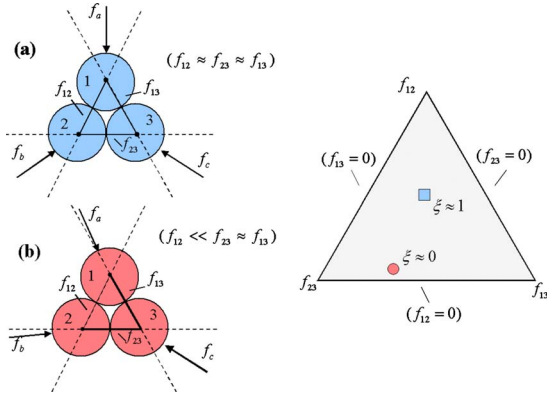
FIG. 9. (Color online) Mapping of loop structures. The stability of a loop can be represented as a function $\xi_{l,3}$ of the contact forces which make it up. (a) Loops with $\xi_{l,3} \approx 1$ (i.e., $f_{12} \approx f_{23} \approx f_{13}$) are very stable and lie near the center of the stable region (represented as a square on the triangular map, at right). (b) Loops with $\xi_{l,3} \approx 0$ (i.e., $f_{12} \ll f_{23} \approx f_{13}$) are marginally stable and lie near the perimeter of the stable region (represented as a circle on the triangular map).

tween tilting and destabilization and identifying additional unique effects of tilting on network structure.

A. Quantifying loop stability

For any contact loop there is a finite range of compatible loads, which corresponds to the allowable set of contact loop forces. Consider a third-order loop, where the contact forces f_{ij}, f_{jk}, and f_{ik}, define the resulting compressive force vectors f_a, f_b, and f_c [see Fig. 9(a)]. The most stable arrangement of contact forces is $f_{ij} = f_{jk} = f_{ik}$, such that each of the resulting compressive force vectors lies in the center of its stable range, and small perturbations in either direction are unlikely to compromise the loop. On the other hand, consider the arrangement $f_{ij} \ll f_{jk} \approx f_{ik}$, for which the compressive force vectors lie near the edge of the stable region [see Fig. 9(b)]. A slight perturbation is likely to move the loop into an unstable region. This loop property is captured with the weighting function ξ:

$$\xi_{l,n} = \frac{1}{\bar{f}^n} \prod_{i=1}^{n} f_i, \qquad (13)$$

where n is the number of edges in the loop and $\bar{f}$ is the mean edge weight, averaged over all the edges in the loop

$$\bar{f} = \frac{1}{n} \sum_{i=1}^{n} f_i. \qquad (14)$$

$\xi_{l,n} = 1$ for a loop with equally weighted edges (the most stable force arrangement) and approaches zero as the relative weight of any edge in a loop goes to zero. For a third order loop, $\xi_{l,3}$ can be mapped onto a two-dimensional space, with the stable region describing an equilateral triangle [see Fig. 9(c)]. $\xi_{l,3} = 1$ lies at the center of the triangle and $\xi_{l,3} = 0$ lies at the perimeter, such that the inner region of the triangle corresponds to greater stability and points lying outside the
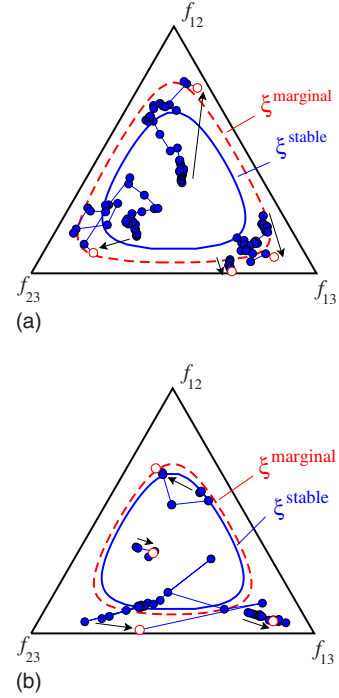

FIG. 10. (Color online) Stability trajectories of individual loops. Trajectories of third-order loops are mapped in the f_{12}, f_{23}, f_{13} triangular stable space for (a) a bed of rough particles ($\mu = 0.5$) and (b) a bed of smooth particles ($\mu = 0$). (Arrows indicate the net trajectory over the life span of the loop.) Filled circles represents a stable stage in the loop trajectory; outlined circles indicate the final, marginally stable stage (after which the loop becomes unstable and fails). In systems with friction, $\xi_{l,3}^s = 0.582 \pm 4 \times 10^{-3}$ (solid blue isostability curve) and $\xi_{l,3}^m = 0.30 \pm 0.02$ (dashed red isostability curve). In frictionless systems, $\xi_{l,3}^s = 0.589 \pm 4 \times 10^{-3}$ and $\xi_{l,3}^m = 0.41 \pm 0.03$.

triangle correspond to unstable configurations. We validate $\xi_{l,3}$ as a stability indicator by mapping its trajectories for individual loops in a gradually tilted bed.

Recall that the granular bed is tilted in intervals (two second tilting interval followed by a two second rest interval). We label the granular network prior to each tilting interval as a stage n such that $n = 1$ corresponds to $\theta_g = 0$, $n = 2$ corresponds to $\theta_g = 0.01$, and so on. This description affords a convenient distinction between stable and marginally stable triples: we say that a triple that exists during stage n is stable if, and only if, it also exists during stage $n+1$. Alternatively, we say that a triple that exists during stage n, but not stage $n+1$ is marginally stable.

Average ξ values for stable ($\xi_{l,3}^s$) and marginally stable ($\xi_{l,3}^m$) triples suggest that ξ is indeed an indicator of loop stability. In our simulations, we find $\xi_{l,3}^s = 0.582 \pm 4 \times 10^{-3}$ and $\xi_{l,3}^m = 0.30 \pm 0.02$ (where the error represents a 95% confidence interval), indicating that marginally stable triples tend to lie nearer to the perimeter of the stable triangle ($\xi_{l,3}^s \approx \xi_{l,3}^m$ would suggest that ξ is a poor indicator of stability). We can visualize the results by plotting $\xi_{l,3}^s$ and $\xi_{l,3}^m$ as isostability curves on the stable triangle [see Fig. 10(a)]. The multistage trajectories of individual triples include several, seemingly random leaps, but have an overall tendency to
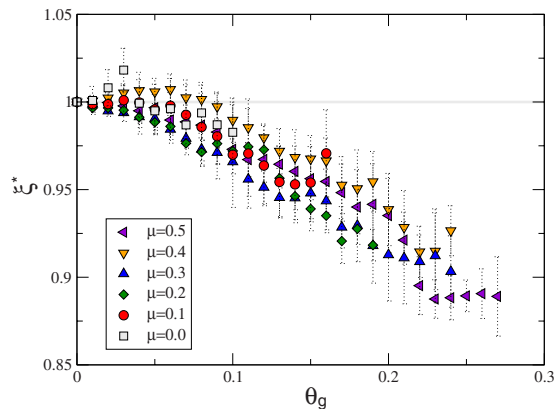
FIG. 11. (Color online) Loop stability as a function of tilting. The normalized mean loop stability ($\xi_{l,3}^*$) tends to decrease as the tilting angle (θ_g) is increased.

migrate toward the outer region of the stable space. In simulations of perfectly smooth particles ($\mu=0$), the difference is less pronounced—$\xi_{l,3}^s=0.589\pm4\times10^{-3}$ and $\xi_{l,3}^m=0.41\pm0.03$ [see Fig. 10(b)].

B. Effects of tilting, revisited

We previously showed that small loops in a granular packing tend to decrease in number as the bed is tilted; according to the quantity ξ, they also decrease in stability. The normalized mean stability of third-order loops

$$\xi_{l,3}^*(\theta_g) = \frac{\langle\xi_{l,3}(\theta_g)\rangle}{\langle\xi_{l,3}(\theta_g=0)\rangle} \qquad (15)$$

can decrease by as much as 15% over the static tilting range (see Fig. 11). This is a unique effect of tilting: mean loop stability in an untilted bed $\langle\xi_{l,3}(\theta_g=0)\rangle$ is roughly independent of contact density (Z), indicating that the tilting effect on loop stability can be isolated from contact density effects [see Fig. 12(a)]. Fourth-order loop stability $\xi_{l,4}$ evolves in a similar manner, although it appears that $\xi_{l,4}$ in the untilted beds may be a weak function of contact density [see Fig. 12(b)].

V. DISCUSSION

It can be argued that the stability of 2D granular packings arises from structures on the order of a few particles, i.e., contact loops. In this paper, we have shown that (1) loop structure in a granular packing is a function of interparticle friction coefficient; (2) granular packings (particularly frictional packings) are especially rich in fourth order loops, compared to a random lattice model; and (3) tilting has unique, destabilizing effects on loop structure.

A natural, if somewhat formidable, extension is to three dimensions. In three dimensions, the smallest structure that can support three-dimensional perturbations of a compressive load is a tetrahedral cluster. However, other such structures exist, including square pyramids, triangular prisms, and
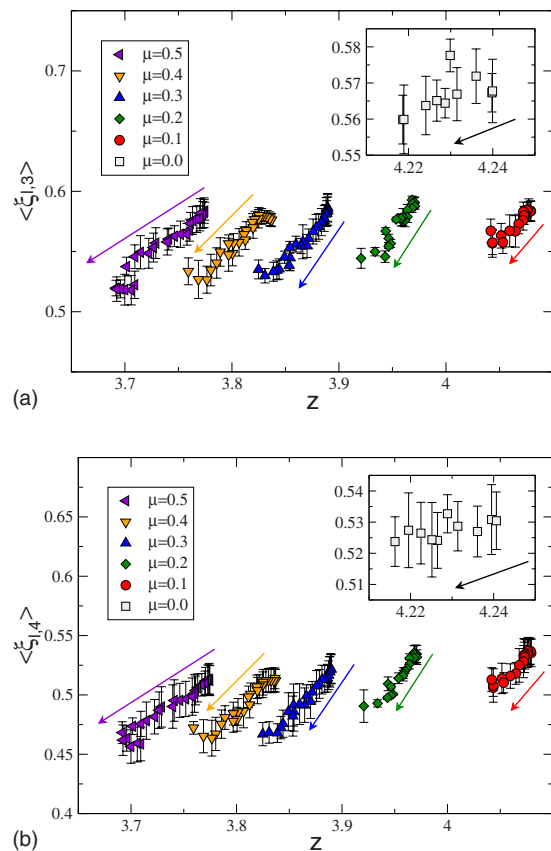

FIG. 12. (Color online) Loop stability and coordination number. (a) Tilting causes a decrease in mean stability of third order loops $\xi_{l,3}$. The untilted values $\xi_{l,3}(\theta_g=0)$ are roughly independent of coordination number, but $\xi_{l,3}$ decreases with increasing tilting angle, suggesting that tilting effects on $\xi_{l,3}$ are unique from contact density effects. (b) Mean stability of fourth order loops $\xi_{l,4}$ evolves in a similar manner. In both (a) and (b), arrows indicate the direction of increasing tilting angle.

cubes, among others. These structures—such as loops in two dimensions—may be viewed as the building blocks for a stable three-dimensional packing, and may influence global stability in three dimensions. (Quantitative indicators analogous to ξ, although possible, would likely be much more complicated in three dimensions.)

However, even in the relatively simple case of a two-dimensional packing, this study has quite possibly raised more questions than it has answered. For example, we have shown that third-order loops tend to migrate from the center of the stable triangular region to the perimeter, and then fail. But where on the perimeter do they most often exit? Near a vertex (i.e., $f_{12}\approx f_{23}\ll f_{13}$) or a midpoint (i.e., $f_{12}\ll f_{23}\approx f_{13}$)? This would be important for understanding failure mechanics. Also, it is well known that forces in a granular packing exhibit spatial organization; are loop structures also spatially organized? Do they destabilize (i.e., $\xi \rightarrow 0$) in clusters, chains, or randomly? These kinds of studies might lead to a better first-principles understanding of stability and fragility in granular packings.

[1] D. Howell, R. Behringer, and C. Veje, Chaos **9**, 559 (1999).

[2] C. Liu, S. Nagel, D. Schecter, S. Coppersmith, S. Majumdar, O. Narayan, and T. Witten, Science **269**, 513 (1995).

[3] H. Jaeger, S. Nagel, and R. Behringer, Rev. Mod. Phys. **68**, 1259 (1996).

[4] M. E. Cates, J. P. Wittmer, J. P. Bouchaud, and P. Claudin, Phys. Rev. Lett. **81**, 1841 (1998).

[5] A. Smart, P. Umbanhowar, and J. Ottino, Europhys. Lett. **79**, 24002 (2007).

[6] S. Deboeuf, O. Dauchot, L. Staron, A. Mangeney, and J. P. Vilotte, Phys. Rev. E **72**, 051305 (2005).

[7] H. A. Makse, N. Gland, D. L. Johnson, and L. Schwartz, Phys. Rev. E **70**, 061302 (2004).

[8] J. N. Roux, Phys. Rev. E **61**, 6802 (2000).

[9] C. F. Moukarzel, Phys. Rev. Lett. **81**, 1634 (1998).

[10] M. Cates, J. Wittmer, J. Bouchaud, and P. Claudin, Chaos **9**, 511 (1999).

[11] N. Rivier, J. Non-Cryst. Solids **352**, 4505 (2006).

[12] R. Arevalo, I. Zuriguel, and D. Maza, eprint arXiv:0709.2680.

[13] R. C. Ball and R. Blumenfeld, Phys. Rev. Lett. **88**, 115505 (2002).

[14] N. Kruyt and L. Rothenburg, Int. J. Solids Struct. **38**, 4879 (2001).

[15] R. Blumenfeld and S. F. Edwards, Phys. Rev. Lett. **90**, 114303 (2003).

[16] J. Schäfer, S. Dippel, and D. Wolf, J. Phys. I **6**, 5 (1996).

[17] P. Cundall and O. Strack, Geotechnique **29**, 47 (1979).

[18] B. Lubachevsky and F. Stillinger, J. Stat. Phys. **60**, 561 (1990).

[19] L. Staron, J. P. Vilotte, and F. Radjai, Phys. Rev. Lett. **89**, 204302 (2002).